IOP Publishing Journal of Physics: Condensed Matter
J. Phys.: Condens. Matter **28** (2016) 305501 (10pp) doi:10.1088/0953-8984/28/30/305501

Quantitative description of short-range order and its influence on the electronic structure in Ag-Pd alloys

M Hoffmann[1,2], A Marmodoro[3], A Ernst[3], W Hergert[2], J Dahl[4,5], J Lång[4,5], P Laukkanen[4,5], M P J Punkkinen[4,5] and K Kokko[4,5]

[1] IFW Dresden, PO Box 270116, D-01171 Dresden, Germany
[2] Institute of Physics, Martin Luther University Halle-Wittenberg, D-06099 Halle, Germany
[3] Max Planck Institute of Microstructure Physics, Weinberg 2, D-06120 Halle, Germany
[4] Department of Physics and Astronomy, University of Turku, FIN-20014 Turku, Finland
[5] Turku University Centre for Materials and Surfaces (MatSurf), Turku, Finland

E-mail: mart.hoffi@gmail.com

Received 3 February 2016, revised 25 April 2016
Accepted for publication 25 April 2016
Published 7 June 2016

Abstract

We investigate the effect of short-range order (SRO) on the electronic structure in alloys from the theoretical point of view using density of states (DOS) data. In particular, the interaction between the atoms at different lattice sites is affected by chemical disorder, which in turn is reflected in the fine structure of the DOS and, hence, in the outcome of spectroscopic measurements. We aim at quantifying the degree of potential SRO with a proper parameter.

The theoretical modeling is done with the Korringa–Kohn–Rostoker Green's function method. Therein, the extended multi-sublattice non-local coherent potential approximation is used to include SRO. As a model system, we use the binary solid solution Ag_cPd_{1-c} at three representative concentrations $c = 0.25$, 0.5 and 0.75. The degree of SRO is varied from local ordering to local segregation through an intermediate completely uncorrelated state. We observe some pronounced features, which change over the whole energy range of the valence bands as a function of SRO in the alloy. These spectral variations should be traceable in modern photoemission experiments.

Keywords: short-range order, first-principles calculations, density of states, photoemission spectroscopy, Ag-Pd, solid solution, KKR

(Some figures may appear in colour only in the online journal)

1. Introduction

Short-range order (SRO), i.e. a partial degree of order within length scales comparable to interatomic distances, affects materials properties in many macroscopic ways. Its effects can be found in the optical conductivity and reflectivity [2, 3], magnetism [4], plasticity [5], and electronic structure [3, 6–9]. A systematic study of SRO in Ag_cPd_{1-c} alloys is particularly informative, because their experimental phase diagram shows continuous solid solubility within the whole concentration range $c \in [0, 1]$, in a randomly substitutional face centered cubic (fcc) structure [10]. Several theoretical predictions of stable long-range order (LRO), i.e. perfectly periodic, lower energy phases, have been also made in this system [1, 11]. These include in particular unit cell types $L1_2$, $L1_1$ and so-called $L1_1^+$ (a variation of the $L1_1$ case, with its original Ag layer hosting 50% Pd atoms [1]) at $c = 0.75$, $c = 0.5$ and $c = 0.25$, respectively (see figure 1).

The present study adds to our previous qualitative investigation of SRO effects on elastic and Fermi surface properties of Ag_cPd_{1-c} [12] a quantitative analysis of various degrees of SRO in Ag_cPd_{1-c}. The theoretical approach used in [12]—the multi-sublattice extension of the dynamical cluster approximation [13] / non-local coherent potential approximation

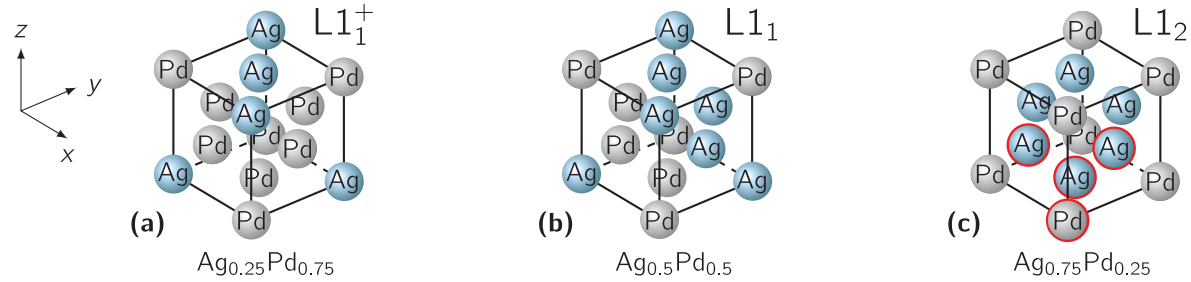

Figure 1. Schematic pictures of the three ordered structures found theoretically by Müller and Zunger [1] for the Ag concentrations $c = 0.25$, 0.5, and 0.75 ((a), (b) and (c), respectively). Only (c) depicts a unit cell (red circles indicate the basis atoms). $L1_1^+$ is formed of a Pd and a mixed Pd/Ag layer in [1 1 1] direction, whereas in $L1_1$, a Pd layer alternates with a full Ag layer in [1 1 1] direction.

(MS-NL-CPA) [14, 15]—extends the original single-site coherent potential approximation (CPA) allowing the evaluation of SRO modeled as local environments up to a given 'cavity' size $N_c \times N_{sub}$. Here, N_{sub} is the number of sublattices in a reference unit cell while N_c counts multiple instances of that unit cell (so-called reciprocal space 'tiles'). The SRO character is then included via the variation of possible occupation of the sublattices by alternative atomic species. It is typically described through the introduction of an order parameter. One example of a SRO parameter, α, is offered by the Warren–Cowley definition [16, 17], which has been previously used for proof-of-concept evaluations of SRO effects in CuZn alloys [14], in comparison with actual neutron scattering experiments on β brass [18], and in the first-principles study of electrical conductivity [19, 20]. Temmermann *et al* [21] found from theoretical calculations that the order-disorder transformation in β brass should be visible in photoemission spectra.

In this work, we further develop such parametrization of the SRO and target a more quantitative comparison with past experiments on Ag_cPd_{1-c} alloys. These alloys are on the one hand easy to handle model systems, since they show intermixing at variable concentrations, but might also stabilize in various geometrically periodic yet substitutionally disordered phases. On the other hand, practical reasons of interest for such compounds are given by possible application for fuel cells, catalysts, hydrogenation, sensors and biosensors and dental implantology [22]. Besides bulk properties, other areas of current interest entail the structure of Pd-Ag nanoparticles (see [23] and references therein).

We calculated the total density of states (DOS) for the different SRO settings and compared the predicted SRO changes with available experimental photoelectron spectroscopy (PES) data. Much more features, which would allow a specific fingerprint of a SRO scenario, were visible in the theoretical prediction than in the measured PES. Since the available experimental material is quite old and the present day high-resolution PES methods will allow better differentiation, we expect that changes in SRO will be traceable within PES experiments.

In the following section 2, we describe the adopted theoretical method in its essential details. The formulation of a suitably general SRO parameter is given in section 2.1. We use it in section 3 to compare between theoretical DOS results at different ordering regimes and the experimental peak positions from PES. Our conclusions are summarized in section 4.

Table 1. Calculated equilibrium lattice constants corresponding to the different alloy concentrations.

c	0.25	0.5	0.75
a_{lat} (Å)	3.890	3.929	3.970

Note: The values are taken from CPA results [12].

2. Computational details

The electronic structure calculation scheme of choice was the Korringa–Kohn–Rostoker Green's function (KKR-GF) method. Here, the HUTSEPOT code developed by Ernst *et al* [24, 25] was used. We adopted the same calculation settings as used in our previous work [12]. Thus, the full charge density approximation (FCDA) was applied in order to describe the potentials properly and the local density approximation (LDA) [26] was used as exchange-correlation functional. The expansion cut-off for the spherical harmonics in the KKR-GF was set to $l_{max} = 3$. Relaxed lattice parameters as a function of the concentration have been computed from total energy minimization through a fit to the Birch–Murnaghan equation of states [27, 28] (table 1).

Within the MS-NL-CPA framework, we describe the SRO considering a multi-site cavity, here set up with $N_c = 1$ tiles but $N_{sub} \geqslant 1$ sublattices [15]. This situation is sketched in figure 2. Beginning from a starting assumption for the coherent medium, the calculation is iterated until self-consistency of the coherent medium. In general, if each disordered cavity site s can host $N_a(s)$ alternative atomic species, there will be in total $N_{tot} = \prod_{s=1}^{N_{sub}} N_a^{N_c}(s)$ possible local configurations γ, each with weight $P(\gamma)$.

This framework allows to recover LRO results when only one, periodically repeated configuration occurs with probability one. On the opposite end, we obtain the fully uncorrelated scenario of a perfectly disordered lattice (which corresponds to the original single-site CPA picture) when all γ are sampled with a probability distribution

$$P(\gamma) = \prod_{I=1}^{N_c} \prod_{s=1}^{N_{sub}} c_{A(I,s,\gamma)}, \quad (1)$$

only given by the factorized concentrations $c_{A(I,s,\gamma)}$. They represent the single-site concentration of an atomic species A appearing on the (MS-)NL-CPA tile $I \in \{1, \ldots, N_c\}$ and the sublattice $s \in \{1, \ldots, N_{sub}\}$, when the cavity is populated by configuration γ. Intermediate scenarios can be described

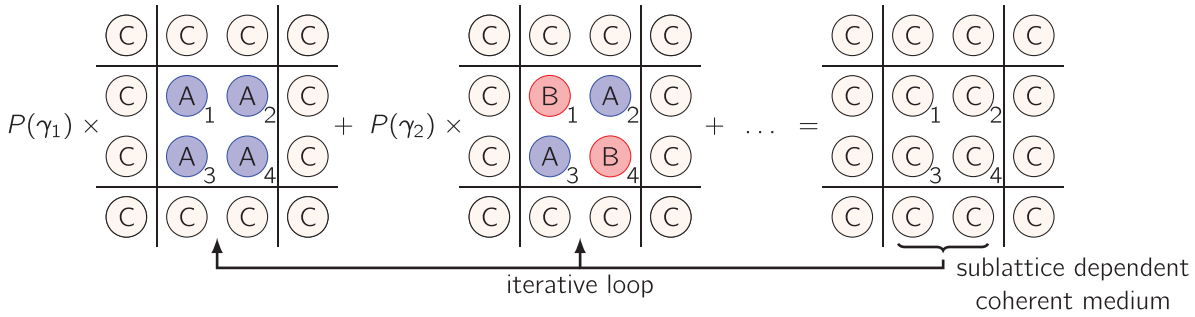

Figure 2. Schematic two-dimensional view of the MS-NL-CPA method for $N_{\mathrm{sub}} = 4$ and $N_{\mathrm{c}} = 1$. Numbers 1–4 mark the sublattice positions s.

adopting alternative probability values $P(\gamma_i) \in [0, 1]$, which are subject to the normalization constraint

$$\sum_{i=1}^{N_{\mathrm{tot}}} P(\gamma_i) = 1, \tag{2}$$

and satisfying the stoichiometry requirement for any atomic type A

$$\frac{1}{N_{\mathrm{c}} N_{\mathrm{sub}}} \sum_{i=1}^{N_{\mathrm{tot}}} P(\gamma_i) \times \mathcal{N}_A(\gamma_i) = c_A. \tag{3}$$

Therein, the factor $\mathcal{N}_A(\gamma_i)$ counts how many atoms of type A appear within configuration γ_i.

We note that our results represent an upper limit for the influence of SRO effects on the physical effective medium, on top of those due to concentration alone. This originates from the N_{c} coarse-graining subdivisions of the original Brillouin zone in reciprocal space [29], which are chosen consistently with the point group symmetries of the lattice but remain only defined up to a systematic offset (or 'tiling phase factor' [29]) in the relative origin for the cluster momenta $\boldsymbol{K}_n$. At the moment, there is no systematic KKR-GF implementation of a corrective, additional sampling step for the tiling phase factor. Therefore, single tiling phase results—such as those discussed in the following—might slightly broaden, when including a proper phase average.

2.1. A general short-range order parameter

We intend to improve our previous work [12] with a quantitative description of SRO, and facilitate a comparison with experiments. To this end, we begin by recalling the Warren–Cowley SRO parameter definition [16, 17]. It is computed for a generic A_c, B_{1-c} binary alloy from the number n_l of A atoms found in the lth shell around a B atom

$$\alpha_l^{BA} = 1 - \frac{n_l}{c_A C_l}, \tag{4}$$

$$= 1 - \frac{p_l^{BA}}{c_A}. \tag{5}$$

Therein, C_l is the coordination number of the lth shell around B and the second expression is obtained by inserting the ratio $p_l^{BA} = n_l/C_l$ of A atoms within shell l around a B atom. Complex unit cell cases can be handled through an additional N_{sub}-normalized summation across sublattices.

When considering a (MS-)NL-CPA cavity, the SRO parameter (4) is deployed for each configuration γ_i, leading to the global result as a $P(\gamma_i)$-weighted average. This general case can present some difficulties, since the shell radius in (4) may exceed the cavity size, so that the occupation of the considered lattice sites lies beyond the explicit listing of a configuration γ_i (see figure 2, colored spheres are 'inside' and C spheres are 'outside' of the cavity). We propose therefore a general SRO parameter defined by the procedure below. Therein, it is convenient to introduce a generic occupation function σ_s^A for each atomic species A, which returns a value '1', if the crystalline position s under examination hosts an A atom, or '0', if not. At every instance, an example is given with respect to the configuration γ_2 in figure 2 (middle panel) with $N_{\mathrm{sub}} = 4$ and $N_{\mathrm{c}} = 1$ (see also section 2.3).

(i) As long as a sublattice remains fully contained within the explicit configuration, the constrained probability for A to appear on sublattice s of the (MS-)NL-CPA cavity cell I is given by the occupation function $\sigma_{I,s}^A$. When instead a shell's site lies beyond the cavity, its constrained probability becomes

$$p_{\mathrm{C}}^A(I, s) = \sum_{i=1}^{N_{\mathrm{tot}}} P(\gamma_i) \sigma_{I,s}^A. \tag{6}$$

We note that in case of a disordered site, in the sense of the single-site CPA, $N_{\mathrm{tot}} = 1$ and the occupation function in (6) is substituted by a concentration.

Example: Sites 1, 2, 3, and 4 are determined by γ_2 (inside the cavity), while all sites marked with C are not included in any configuration (outside the cavity).

(ii) The conditional probability in (5) for each configuration γ_i and across the shell l is computed by

$$p_l^{BA}(\gamma_i, I, s) = \frac{1}{C_l} \sum_{n=1}^{C_l} \begin{cases} p_{\mathrm{C}}^A(I, s) & n \text{ outside}, \\ \sigma_{I,s}^A & n \text{ inside}, \end{cases} \tag{7}$$

where the $n = 1, \ldots, C_l$ sites are either inside or outside the cavity.

Example: Site 1 has four nearest neighbor sites. The probability of sites 2 and 3 is taken into account within γ_2

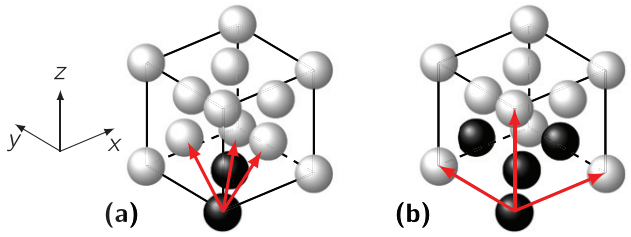

Figure 3. The used cells for the representation of the fcc lattice. (a) with two basis sites. (b) with 4 basis sites. Red arrows indicate the lattice vectors, and black spheres represent the basis sites.

by $\sigma^A_{1,2}$ and $\sigma^A_{1,3}$, respectively, whereas the other two sites are outside and their probability is $p^A_C(1,2)$ and $p^A_C(1,3)$.

(iii) Using (7) in (5) yields the SRO parameter $\bar{\alpha}_l(\gamma_i)$ as a function of the configuration γ_i. The arithmetic average is taken over all sublattices and tiles for the lth shell (using $\alpha^{AB}_l(\gamma_i, I, s)$ or $\alpha^{BA}_l(\gamma_i, I, s)$).

Example: Average over the sites 1, 2, 3 and 4.

(iv) In a final step, the SRO parameter per shell is derived via

$$\alpha_l = \sum_{i=1}^{N_{\text{tot}}} P(\gamma_i) \times \bar{\alpha}_l(\gamma_i). \tag{8}$$

Example: Take into account all other configurations and the corresponding $P(\gamma_i)$ as well.

(v) A possible average over the shells up to N_{sh} may include weighting with the coordination number C_l [30]

$$\langle\alpha\rangle_{N_{\text{sh}}} = \left[\sum_{l=1}^{N_{\text{sh}}} C_l \times \alpha_l\right] \Big/ \sum_{l=1}^{N_{\text{sh}}} C_l. \tag{9}$$

However, N_{sh} is not yet defined. Its value may depend on the lattice structure as discussed below in section 3.2. Thus, we restrict this study to the nearest neighbor SRO parameter.

2.2. Parameter space of the probabilities: an example

Although the definition of the SRO parameter consists only of different kinds of averages, the determination of the input probabilities is still an open question [31]. The connection of the SRO parameter with the probabilities can be only visualized for a simple test case, which contains only $N_{\text{sub}} = 2$ sublattices with $N_{\text{tot}} = 2^2 = 4$ possible configurations. Otherwise, the number of configurations becomes too large. Therefore, we begin at first to consider this $N_{\text{sub}} = 2$ example for a lattice, which is described by the vectors $\boldsymbol{R}_1 = (0, 1/2, 1/2)$, $\boldsymbol{R}_2 = (1/2, 0, 1/2)$ and $\boldsymbol{R}_3 = (1, 1, 0)$ and the basis vectors $\boldsymbol{a}_1 = (0, 0, 0)$ and $\boldsymbol{a}_2 = (1/2, 1/2, 0)$ (see figure 3(a)). This lattice structure resembles an fcc lattice.

The system of equations formed from (2) and (3) has only one solution and yields for the four probabilities

$$P(\gamma_1) = P(\gamma_4). \tag{10}$$

$$P(\gamma_2) = 1 - P(\gamma_3) - 2P(\gamma_4). \tag{11}$$

$$0 \leqslant P(\gamma_3) \leqslant 1. \tag{12}$$

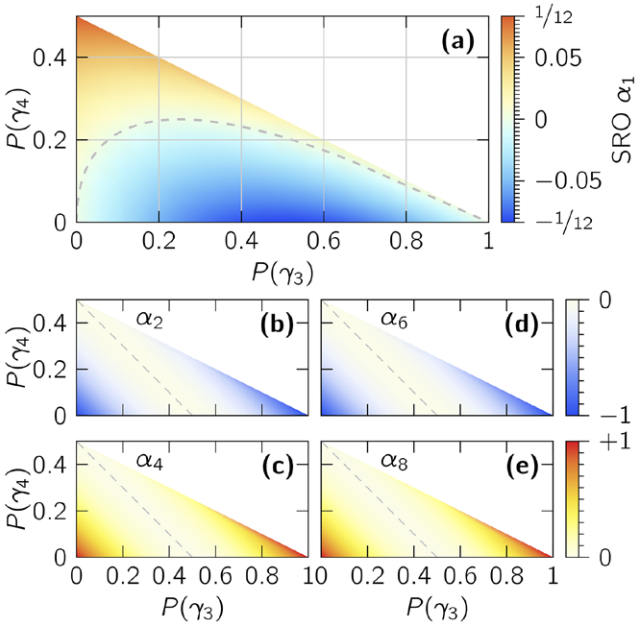

Figure 4. (a) The nearest neighbor SRO parameter α_1, color coded as a function of the two probabilities $P(\gamma_3) = P(\text{Pd Ag})$ and $P(\gamma_4) = P(\text{Pd Pd})$. The triangle shape follows from the restrictions in (12) and (13). The dashed line indicates $\alpha_1 = 0$. (b)–(e) The SRO parameter for the following shells vary between −1 and 1 and repeat themselves (see text). The SRO parameter not shown (α_3, α_5, α_7) are completely zero.

$$0 \leqslant P(\gamma_4) \leqslant \frac{1 - P(\gamma_3)}{2}. \tag{13}$$

The two latter probabilities are free parameters. These allow a graphical analysis of the SRO parameter in a contour plot (see figure 4). The local variations inside the cavity determines only the nearest neighbor SRO parameter α_1 (see figure 4(a)). It varies between $-\frac{1}{12}$ and $+\frac{1}{12}$. The highest degree of order is found for $P(\gamma_3) = 0.5$ and $P(\gamma_4) = 0$, which means having the configurations (Pd Ag) and (Ag Pd) equally distributed. On the other hand, the highest degree of segregation in α_1 is realized having $P(\gamma_1) = P(\gamma_4) = 0.5$.

The higher shells reflect the periodicity of the underlying lattice and the coherent medium (see figures 4(b)–(e)). Due to the choice of the lattice and basis vectors, the first period includes the shells until $l = 5$. However, we restrict in this study the average of the SRO parameter to the non-periodic contribution, since this represents mainly the character of the SRO.

2.3. A reasonable choice of sublattices

Although the example demonstrates well the concept of the SRO parameter in the MS-NL-CPA, its configuration space is a little bit too restricted. Therefore, we considered a $N_{\text{sub}} = 4$, $N_c = 1$, cavity supercell sketched in figure 3(b) (lattice vectors of a simple cubic cell with the basis of $\boldsymbol{a}_1 = (0, 0, 0)$, $\boldsymbol{a}_2 = (1/2, 1/2, 0)$, $\boldsymbol{a}_3 = (1/2, 0, 1/2)$ and $\boldsymbol{a}_4 = (0, 1/2, 1/2)$). In this case, the corresponding probabilities of the $N_{\text{tot}} = 2^4 = 16$ configurations can not be parametrized by two free values.

Table 2. All 16 possibilities for the occupation of $N_{\text{sub}} = 4$ sublattices in fcc Ag_cPd_{1-c}.

	Configurations γ_i							
i	$\boldsymbol{a}_1$	$\boldsymbol{a}_2$	$\boldsymbol{a}_3$	$\boldsymbol{a}_4$	c_{Ag}	c_{Pd}	$\mathcal{N}_{\text{Ag}}(\gamma_i)$	
1	Ag	Ag	Ag	Ag	1	0	4	$\tilde{P}(4)$
2	Ag	Ag	Ag	Pd	$\frac{3}{4}$	$\frac{1}{4}$	3	$\tilde{P}(3)$
3	Ag	Ag	Pd	Ag	$\frac{3}{4}$	$\frac{1}{4}$	3	
4	Ag	Pd	Ag	Ag	$\frac{3}{4}$	$\frac{1}{4}$	3	
5	Pd	Ag	Ag	Ag	$\frac{3}{4}$	$\frac{1}{4}$	3	
6	Ag	Ag	Pd	Pd	$\frac{1}{2}$	$\frac{1}{2}$	2	$\tilde{P}(2)$
7	Ag	Pd	Ag	Pd	$\frac{1}{2}$	$\frac{1}{2}$	2	
8	Ag	Pd	Pd	Ag	$\frac{1}{2}$	$\frac{1}{2}$	2	
9	Pd	Ag	Ag	Pd	$\frac{1}{2}$	$\frac{1}{2}$	2	
10	Pd	Ag	Pd	Ag	$\frac{1}{2}$	$\frac{1}{2}$	2	
11	Pd	Pd	Ag	Ag	$\frac{1}{2}$	$\frac{1}{2}$	2	
12	Ag	Pd	Pd	Pd	$\frac{1}{4}$	$\frac{3}{4}$	1	$\tilde{P}(1)$
13	Pd	Ag	Pd	Pd	$\frac{1}{4}$	$\frac{3}{4}$	1	
14	Pd	Pd	Ag	Pd	$\frac{1}{4}$	$\frac{3}{4}$	1	
15	Pd	Pd	Pd	Ag	$\frac{1}{4}$	$\frac{3}{4}$	1	
16	Pd	Pd	Pd	Pd	0	1	0	$\tilde{P}(0)$

Note: The last column defines the new probabilities $\tilde{P}(\mathcal{N}_{\text{Ag}}(\gamma_i))$.

However, the restrictions in (2) and (3) depend only on the number of A or B types in each configuration (internal concentration), whereby several configurations have an equal number of atomic types, which occupy only different sublattices (see table 2). A new probability $\tilde{P}(\mathcal{N}_{\text{Ag}}(\gamma_i))$ is assigned to every group depending on the number of Ag atoms $\mathcal{N}_{\text{Ag}}(\gamma_i)$. With these 5 probabilities, the system of equations (2) and (3) can be solved again, where two probabilities are determined by the others (see appendix A). In fact, each $\tilde{P}(\mathcal{N}_{\text{Ag}}(\gamma_i))$ describes a subset of configurations, e.g. $\tilde{P}(3)$ condenses four configurations (γ_2 to γ_5), each having one Pd occupying another sublattice while the three sublattices left are occupied with Ag. Then, the probabilities $P(\gamma_2)$, $P(\gamma_3)$, $P(\gamma_4)$, and $P(\gamma_5)$ are free to choose but have to sum up to $\tilde{P}(3)$, otherwise violating the total concentration.

2.4. Comparison with experimental PES

We compare below our calculations of the DOS for different SRO regimes with experimental valence band PES of Ag-Pd alloys by McLachlan *et al* [32]. The mean positions of the experimentally observed spectral peaks are considered as the electron binding energies and are given in table 3. We preferred in particular the experimental He II (40.81 eV) spectra. Although the He II technique is in general rather surface sensitive, we expect that its application to metals with a highly efficient electronic screening can lead to useful insights on the bulk properties from analysis of the spectra. This is further confirmed by comparison of the specific He II results used in this study against the calculated XPS spectra of Winter *et al* [33], and the typical probing depth of about 50 Å reported in experiments by Caroli *et al* [34], thus including substantial bulk contributions.

Table 3. Binding energies (in eV, relative to the Fermi energy) of the main spectral peaks estimated from the experimental (He II) spectra by McLachlan *et al* [32] and interpolated to the concentrations used in the present calculations.

$Ag_{0.25}Pd_{0.75}$	$Ag_{0.50}Pd_{0.50}$	$Ag_{0.75}Pd_{0.25}$
0.5	1.0	1.4
2.4	2.3	—
4.9	4.6	4.4
5.5	5.7	6.0

Note: The upper two rows are for the Pd 4*d* section of the spectrum and the lower two rows belong to the Ag 4*d* section.

3. Results

3.1. Broadening of the theoretical spectrum

When comparing theoretical DOS data with experimental results, the experimental resolution broadens the measured spectra and may hide some spectral features. The experimental resolution in the study of McLachlan *et al* [32] is given by ±0.3 eV. However, in the modern high-resolution photoelectron measurement equipment, the energy resolution can go down to the range of few meV at low temperatures around 10 K [35, 36]. The influence of the experimental resolution on the calculated DOS can be simulated by the convolution of the DOS with a Gaussian. The resolution is understood as the full width at half maximum (FWHM) and is translated to the standard deviation σ of the Gaussian distribution by $\text{FWHM} = 2\sqrt{2\ln 2}\,\sigma$.

For two extreme SRO regimes, $\alpha_1 = 0$ (totally uncorrelated) and the $L1_1$ structure (order), the calculated and broadened DOS are depicted in figure 5. The first choice of $\text{FWHM} = 0.6$ (red solid lines) corresponds to the resolution of the older experiment [32], whereas the $\text{FWHM} = 0.2$ (light blue lines) matches with modern resolutions at room temperature. Already the latter resolution is sufficient to represent all significant peaks in the calculated DOS (black dashed line), even for the spiky DOS of the ordered structure (see figure 5(b)). It shows that this resolution would be in principle enough to differentiate between different SRO regimes with the combination of first-principles calculations and PES measurements. This is difficult with the older resolution, since the number of peaks and their variation is hardly distinguishable for the two examples $\alpha_1 = 0$ and $L1_1$ (compare red lines in figure 5). A comparison with the experimental peak position (see table 3) does not reveal a clear conclusion about the particular state of order.

3.2. Varying the short-range order

As a second step, we varied the degree of SRO at the Ag_cPd_{1-c} alloy concentrations $c = 0.25, 0.50, 0.75$. We started with only

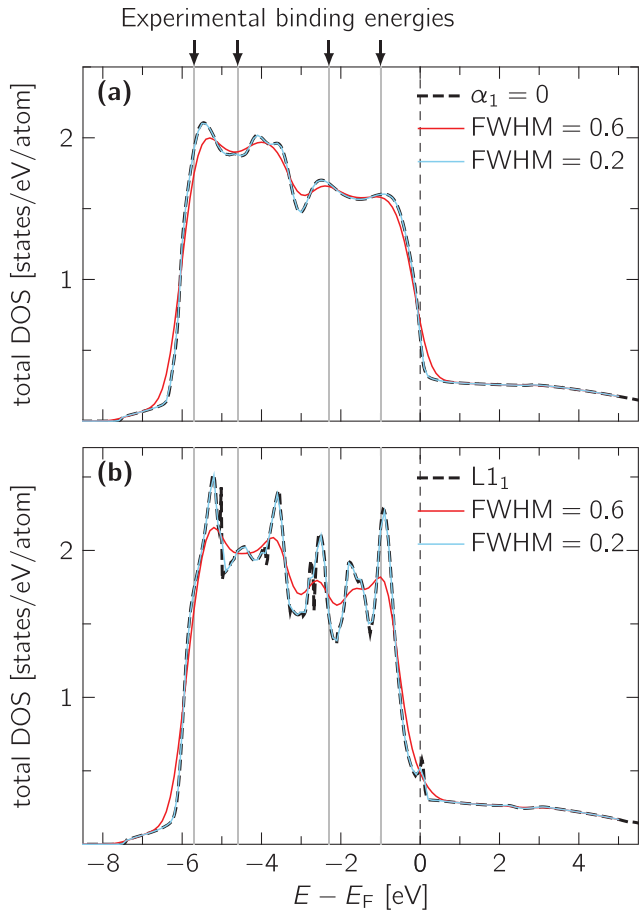

Figure 5. Calculated density of states of $Ag_{0.5}Pd_{0.5}$ convoluted with a Gaussian of different FWHM in order to simulate the experimental resolution. Two cases of SRO are depicted (a) $\alpha_1 = 0$ and (b) the ordered $L1_1$ structure. The binding energies of the main spectral peaks of the experimental PES (table 3) are highlighted by arrows and vertical gray lines. The spectra for the high experimental resolution (FWHM = 0.2, blue line) and the purely theoretical spectra (black dashed line) lie almost on top of each other.

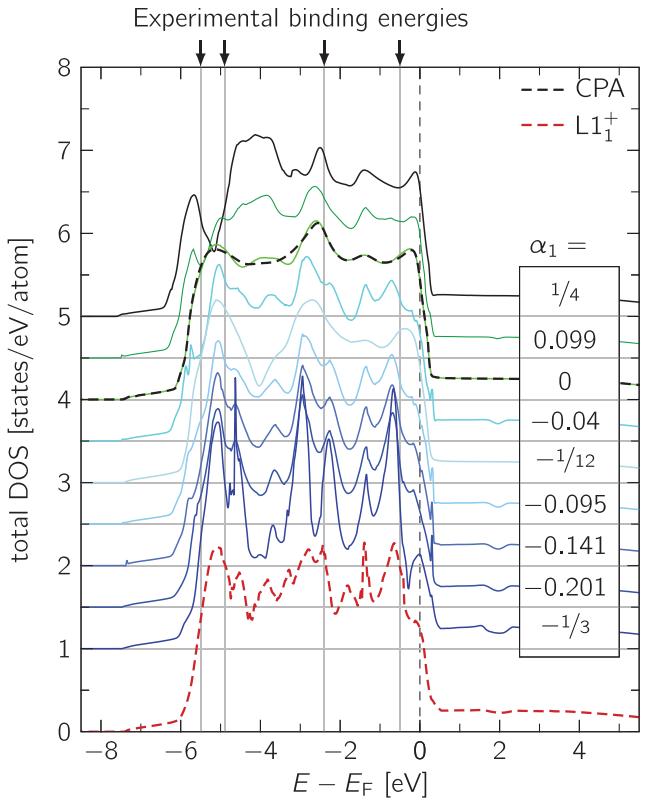

Figure 6. Calculated density of states of $Ag_{0.25}Pd_{0.75}$ for different degrees of nearest neighbor SRO α_1, beginning with the ordered $L1_1^+$ structure. The corresponding configurations used for the SRO parameter are given in table B1. An offset is added to the curves (horizontal gray line represents zero). The binding energies of the main spectral peaks of the experimental PES (table 3) are highlighted by arrows and vertical gray lines.

5 representative configurations of table 2, in particular 1, 2, 6, 12, 16, and varied the three probabilities, which are the free parameters (see appendix A), in steps of 0.05. The obtained SRO parameter showed again a periodicity as already discussed in section 2.2. We chose several SRO parameter values and calculated the valence DOS. The results in dependence of the nearest neighbor SRO parameter α_1 and for the ordered structures are depicted in figures 6–8, respectively. The three figures show significant changes in the DOS with varying SRO. Some spectral peaks vanish, move or grow. Such strong variations should be easily visible in nowadays PES measurements.

When going from the ordered regime ($\alpha_1 < 0$) via the totally uncorrelated case ($\alpha_1 = 0$) towards the segregation regime ($\alpha_1 > 0$), the spiky structure of the DOS looses its contrast and becomes smoother. Simultaneously, the band width is enhanced with increasing α_1. Additionally, the experimental binding energies (see table 3) are indicated within the figures 6–8 with arrows and thin gray lines. Although it became obvious in section 3.1 that a direct comparison between the experimental and theoretical results is hardly possible, the binding energies can at least be related with some pronounced peaks in the DOS and may offer a crude estimation of possible SRO scenarios.

For $Ag_{0.25}Pd_{0.75}$, the best agreement with the binding energies would be achieved with the assumption of a slight tendency of SRO around $\alpha_1 = 0$, since the double peak structure of the binding energies in the lower energy spectrum may hint to additional features coming from SRO (see figure 6). Nevertheless, the variation in the amount of SRO in $Ag_{0.25}Pd_{0.75}$ visualizes the gradually collapse or development of several spectral peaks when going from negative to positive α_1. The minimal value for α_1 is $-\frac{1}{3}$ and represents again the $L1_2$ structure (but now, Ag atoms at the corners and Pd atoms at the faces of the cube). In contrast, $L1_1^+$ was found to be energetically more favorable but has a lower degree of ordering in terms of α_1 ($\alpha_1 = -\frac{1}{9}$, $\alpha_2 = -\frac{1}{3}$, $\alpha_3 = -\frac{1}{9}$, ...). The averaged SRO parameters are $\langle\alpha\rangle_2 = -\frac{5}{27} \approx -0.185$ or $\langle\alpha\rangle_3 = -\frac{1}{7} \approx -0.143$. The different amount of SRO in $L1_2$ or $L1_1^+$ is directly visible in the DOS of both structures (see the dark blue line or the red dashed line in figure 6). While the DOS of $L1_2$ ($\alpha_1 = -\frac{1}{3}$) yielded sharper spectral peaks, the DOS of $L1_1^+$ matches better between $\alpha_1 = -0.141$ and $\alpha_1 = -0.201$.

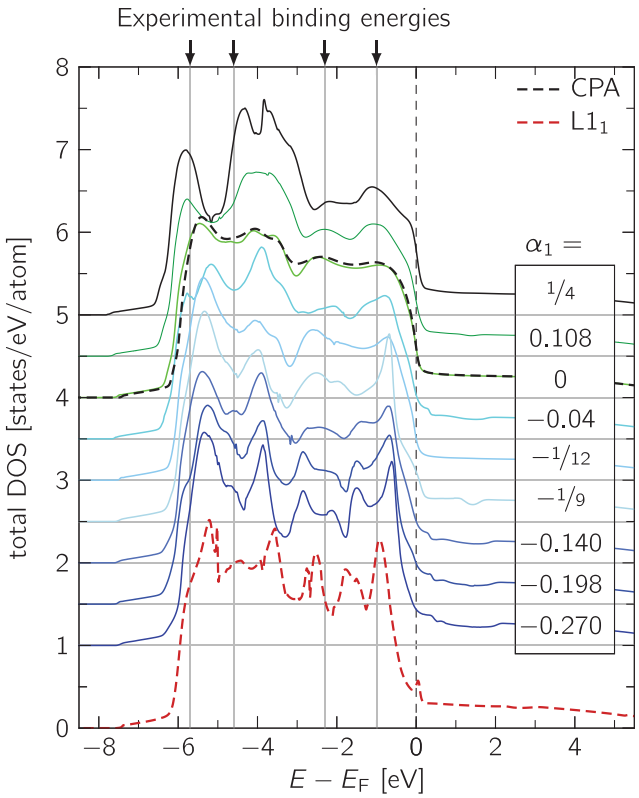

Figure 7. Calculated density of states of $Ag_{0.5}Pd_{0.5}$ for different degrees of nearest neighbor SRO α_1, beginning with the ordered $L1_1$ structure. The corresponding configurations used for the SRO parameter are given in table B2. An offset is added to the curves (horizontal gray line represents zero). The binding energies of the main spectral peaks of the experimental PES (table 3) are highlighted by arrows and vertical gray lines.

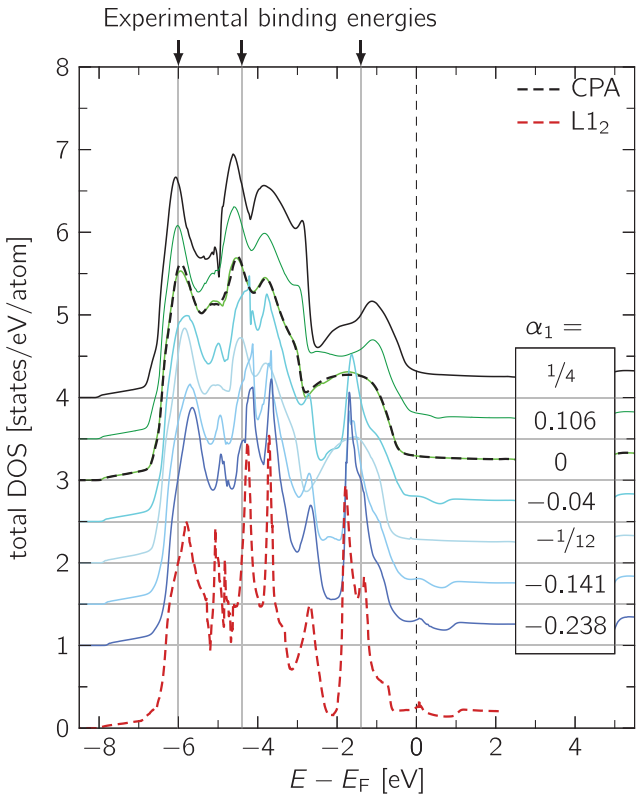

Figure 8. Calculated density of states of $Ag_{0.75}Pd_{0.25}$ for different degrees of nearest neighbor SRO α_1, beginning with the ordered $L1_2$ structure. The corresponding configurations used for the SRO parameter are given in table B3. An offset is added to the curves (horizontal gray line represents zero). The binding energies of the main spectral peaks of the experimental PES (table 3) are highlighted by arrows and vertical gray lines.

The analysis of the DOS for $Ag_{0.5}Pd_{0.5}$ is quite similar as for $Ag_{0.25}Pd_{0.75}$. Several spectral peaks become wider and shift their positions (see figure 7). Also for this concentration, the proposed ordered structure $L1_1$ has not the lowest possible SRO parameter (minimum is $\alpha_1 = -1$, but for $L1_1$ is $\alpha_1 = 0$, $\alpha_2 = -1$, $\alpha_3 = 0$, $\alpha_4 = 1$, ...). The DOS does not seem to fit well in respect of the other DOS of the remaining SRO scenarios. The symmetric cubic cell with $N_{sub} = 4$ might not be the best choice of comparing with the layered structure of $L1_1$. In terms of the experimental binding energies, the SRO regime of $\alpha_1 = 0$ agrees best with the theoretically calculated number of spectral peaks and their positions.

When further raising the concentration of Ag to $Ag_{0.75}Pd_{0.25}$, the SRO related widening of the spectral peaks observed for the ordered structure $L1_2$ can be traced (see energy range between -2 eV to 0 eV in figure 8). $L1_2$ ($\alpha_1 = -\frac{1}{3}$) has already the lowest possible SRO parameter and is described well by the small cubic cell. Thus, all spectral peaks obtained for $L1_2$ just loose their height and become broader, if the SRO is varied towards $\alpha_1 = 0$. The comparison with the experimental binding energies at $c = 0.75$ indicates again a mostly disordered sample representing the crucial peaks in the theoretical spectrum well (see arrows in figure 8).

The good description of the $c = 0.75$ case within the $N_{sub} = 4$ supercell (see figure 3) is also verified by calculated total energies. Thereby, the $L1_2$ structure had the lowest total energy and the total energy increased just linearly (not shown) when varying the degree of SRO. However for the other two concentrations, there was no clear tendency visible. Only the respective ordered structures—$L1_1$ and $L1_1^+$—had the lowest total energies.

Finally, the calculated DOS at $c = 0.25$, 0.5 and 0.75 were also compared with the PES measurements of Norris and Nilsson [37], Hüfner *et al* [38, 39], Chae *et al* [40] and Traditi *et al* [41]. In general, the experimental spectra agree best with the DOS of the random ($\alpha_1 = 0$) or the ordering ($\alpha_1 < 0$) cases, while the clustering features ($\alpha_1 > 0$) are less probable. This is in agreement with the complete solubility of Ag and Pd at ambient temperatures and with the ordering tendency at low temperatures [1].

Table B1. Nearest neighbor SRO parameter and the corresponding configurations used for fcc $Ag_{0.25}Pd_{0.75}$ with $N_{sub} = 4$.

		Probabilities $P(\gamma_i)$ for $\alpha_1 =$							
Confs.	c_{Ag}	$-\frac{1}{3}$	−0.201	−0.141	−0.095	$-\frac{1}{12}$	−0.04	0.099	$\frac{1}{4}$
1 1 1 1	1	0	0	0.05	0.05	0	0.1	0.15	$\frac{1}{4}$
1 1 1 0	$\frac{3}{4}$	0	0.05	0	0.05	0	0	0	0
1 1 0 0	$\frac{1}{2}$	0	0.05	0.05	0	0	0	0.05	0
1 0 0 0	$\frac{1}{4}$	1	$\frac{3}{4}$	0.7	0.65	$\frac{1}{4}$	0.6	0.3	0
0 1 0 0	$\frac{1}{4}$	0	0	0	0	$\frac{1}{4}$	0	0	0
0 0 1 0	$\frac{1}{4}$	0	0	0	0	$\frac{1}{4}$	0	0	0
0 0 0 1	$\frac{1}{4}$	0	0	0	0	$\frac{1}{4}$	0	0	0
0 0 0 0	0	0	0.15	0.2	$\frac{1}{4}$	0	0.3	$\frac{1}{2}$	$\frac{3}{4}$

Note: For $\alpha = 0$, all 16 configurations are used and their probabilities are given by (1).

4. Conclusions

The SRO induced changes in the DOS are significantly larger than the typical energy resolution in the valence band PES measurements [32]. We have demonstrated that the SRO phenomena in alloys can be in principle discernible in valence band photoelectron spectra. With proper SRO calculations, e.g. within the MS-NL-CPA, the experimental PES data can be used to determine the type of the prevailing SRO. Thus, the PES technique can be considered as one potential experimental method to investigate SRO structures of alloys.

Comparing our MS-NL-CPA valence DOS of Pd-Ag alloys with existing PES measurements suggests that the SRO in the measured Pd-Ag samples has been in most cases that of uncorrelated disorder with some traces of local ordering. Nevertheless, PES measurements with resolution available in modern technique would be beneficial to get more definite information of SRO in Pd-Ag alloys.

Acknowledgments

This work was partially funded by the Deutsche Forschungsgemeinschaft (DFG) within SFB 762, Functionality of Oxide Interfaces. We gratefully acknowledge financial support by the Deutscher Akademischer Austauschdienst (DAAD) and the Academy of Finland (Grant No. 134270).

Appendix A. Relation between probabilities

The redefined probabilities $\tilde{P}(\mathcal{N}_{Ag}(\gamma_i))$ form a similar system of equations as (2) and (3)

$$\tilde{P}(4) + \frac{3}{4}\tilde{P}(3) + \frac{1}{2}\tilde{P}(2) + \frac{1}{4}\tilde{P}(1) = c, \tag{A.1}$$

$$\frac{1}{4}\tilde{P}(3) + \frac{1}{2}\tilde{P}(2) + \frac{3}{4}\tilde{P}(1) + \tilde{P}(0) = 1 - c, \tag{A.2}$$

$$\sum_i^4 \tilde{P}(i) = 1, \tag{A.3}$$

$$0 \leqslant \tilde{P}(i) \leqslant 1, \tag{A.4}$$

where $c = c_{Ag}$ and $1 - c = c_{Pd}$. This system of equations has, in particular for $c = 0.5$, a solution where the parameter space is spanned by $\tilde{P}(2)$, $\tilde{P}(3)$, and $\tilde{P}(4)$, under the conditions

$$\begin{aligned}&(2\tilde{P}(2) + 3\tilde{P}(3) + 4\tilde{P}(4) \leqslant 2)\\ &\bigwedge\{[(\tilde{P}(2) + 2\tilde{P}(3) + 3\tilde{P}(4) \geqslant 1) \wedge (\tilde{P}(2) + 2\tilde{P}(3) \leqslant 1)]\\ &\bigvee[(\tilde{P}(2) + 2\tilde{P}(3) \geqslant 1) \wedge (2\tilde{P}(2) + 3\tilde{P}(3) \leqslant 2)]\}.\end{aligned} \tag{A.5}$$

The remaining probabilities are then given by

$$\tilde{P}(0) = \tilde{P}(2) + 2\tilde{P}(3) + 3\tilde{P}(4) - 1, \tag{A.6}$$

$$\tilde{P}(1) = 2 - 2\tilde{P}(2) - 3\tilde{P}(3) - 4\tilde{P}(4). \tag{A.7}$$

If $\tilde{P}(4)$ is zero, a simple solution follows from (A.5)

$$\tilde{P}(0) = \frac{1 - \tilde{P}(2)}{3}, \tag{A.8}$$

$$\tilde{P}(1) = \tilde{P}(4) = 0, \tag{A.9}$$

$$\tilde{P}(3) = -\frac{2(\tilde{P}(2) - 1)}{3}, \tag{A.10}$$

while $0 \leqslant \tilde{P}(2) \leqslant 1$ is the only free parameter. The conditions and probabilities for the other concentrations $c = 0.25$ and 0.75 can be found following a similar procedure.

Appendix B. Used configurations and probabilities

The configurations and probabilities used to calculate the DOS shown in figures 6–8 are presented in tables B1, B2, and B3, respectively. Besides, the 5 representative configurations indicated in table 2, we chose also additional configurations in order to test the method.

Table B2. Nearest neighbor SRO parameter and the corresponding configurations used for fcc $Ag_{0.5}Pd_{0.5}$ with $N_{sub} = 4$.

		Probabilities $P(\gamma_i)$ for $\alpha_1 =$							
Confs.	c_{Ag}	−0.270	−0.198	−0.140	$-\frac{1}{9}$	$-\frac{1}{12}$	−0.04	0.108	$\frac{1}{4}$
1 1 1 1	1	0	0.1	0	0	0	0.2	0.3	$\frac{1}{2}$
1 1 1 0	$\frac{3}{4}$	0.05	0	0.15	0	0	0	0.1	0
1 1 0 1	$\frac{3}{4}$	0.05	0	0.15	0	0	0	0	0
1 1 0 0	$\frac{1}{2}$	0.8	0.7	0.5	0	$\frac{1}{6}$	0.6	0.2	0
1 0 1 0	$\frac{1}{2}$	0	0	0	0	$\frac{1}{6}$	0	0	0
1 0 0 1	$\frac{1}{2}$	0	0	0	$\frac{1}{3}$	$\frac{1}{6}$	0	0	0
0 1 1 0	$\frac{1}{2}$	0	0	0	0	$\frac{1}{6}$	0	0	0
0 1 0 1	$\frac{1}{2}$	0	0	0	$\frac{1}{3}$	$\frac{1}{6}$	0	0	0
0 0 1 1	$\frac{1}{2}$	0	0	0	$\frac{1}{3}$	$\frac{1}{6}$	0	0	0
1 0 0 0	$\frac{1}{4}$	0.1	0.2	0.1	0	0	0	0.1	0
0 0 0 0	0	0	0	0.1	0	0	0.2	0.3	$\frac{1}{2}$

Note: For $\alpha = 0$, all 16 configurations are used and their probabilities are given by (1).

Table B3. Nearest neighbor SRO parameter and the corresponding configurations used for fcc $Ag_{0.75}Pd_{0.25}$ with $N_{sub} = 4$.

		Probabilities $P(\gamma_i)$ for $\alpha_1 =$					
Confs.	c_{Ag}	−0.238	−0.141	$-\frac{1}{12}$	−0.04	0.106	$\frac{1}{4}$
1 1 1 1	1	0.1	0.2	0	0.3	0.6	$\frac{3}{4}$
1 1 1 0	$\frac{3}{4}$	0.85	0.7	$\frac{1}{4}$	0.6	0.1	0
1 1 0 1	$\frac{3}{4}$	0	0	$\frac{1}{4}$	0	0	0
1 0 1 1	$\frac{3}{4}$	0	0	$\frac{1}{4}$	0	0	0
0 1 1 1	$\frac{3}{4}$	0	0	$\frac{1}{4}$	0	0	0
1 1 0 0	$\frac{1}{2}$	0	0.05	0	0	0.05	0
1 0 0 0	$\frac{1}{4}$	0.05	0	0	0	0.2	0
0 0 0 0	0	0	0.05	0	0.1	0.05	$\frac{1}{4}$

Note: For $\alpha = 0$, all 16 configurations are used and their probabilities are given by (1).

References

[1] Müller S and Zunger A 2001 *Phys. Rev. Lett.* **87** 165502
[2] Mookerjee A, Tarafder K, Chakrabarti A and Saha K K 2008 *Pramana* **70** 221
[3] Jezierski A 1993 *Phys. Status Solidi* b **178** 373
[4] Parra R E and González A C 1999 *J. Appl. Phys.* **85** 4735
[5] Jiang M and Dai L 2010 *Phil. Mag. Lett.* **90** 269
[6] Staunton J B, Johnson D D and Pinski F J 1994 *Phys. Rev.* B **50** 1450
[7] Wahrenberg R, Stupp H, Boyen H G and Oelhafen P 2000 *Europhys. Lett.* **49** 782
[8] Golovchak R, Shpotyuk O, Kozyukhin S, Shpotyuk M, Kovalskiy A and Jain H 2011 *J. Non-Cryst. Solids* **357** 1797
[9] Novikov Y N and Gritsenko V A 2011 *J. Appl. Phys.* **110** 014107
[10] Hultgren R, Desai P D, Hawkins D T, Gleiser M and Kelley K K 1973 *Selected Values of the Thermodynamic Properties of Binary Alloys* (Metals Park, OH: American Society for Metals)
[11] Ruban A V, Simak S I, Korzhavyi P A and Johansson B 2007 *Phys. Rev.* B **75** 054113
[12] Hoffmann M, Marmodoro A, Nurmi E, Kokko K, Vitos L, Ernst A and Hergert W 2012 *Phys. Rev.* B **86** 094106
[13] Jarrell M and Krishnamurthy H R 2001 *Phys. Rev.* B **63** 125102
[14] Rowlands D A, Ernst A, Györffy B L and Staunton J B 2006 *Phys. Rev.* B **73** 165122
[15] Marmodoro A, Ernst A, Ostanin S and Staunton J B 2013 *Phys. Rev.* B **87** 125115
[16] Cowley J M 1950 *Phys. Rev.* **77** 669
[17] Warren B E 1990 *X-ray Diffraction* (New York: Dover)
[18] Walker C B and Keating D T 1963 *Phys. Rev.* **130** 1726
[19] Butler W H and Stocks G M 1984 *Phys. Rev.* B **29** 4217
[20] Lowitzer S, Ködderitzsch D, Ebert H, Tulip P R, Marmodoro A and Staunton J B 2010 *Europhys. Lett.* **92** 37009
[21] Temmerman W M, Durham P J, Szotek Z, Sob M and Larsson C G 1988 *J. Phys. F: Met. Phys.* **18** 2387
[22] Li D, Baba N, Brantley W A, Alapati S B, Heshmati R H and Daehn G S 2010 *J. Mater. Sci., Mater. Med.* **21** 2723
[23] Kozlov S M, Kovács G, Ferrando R and Neyman K M 2015 *Chem. Sci.* **6** 3868
[24] Ernst A 2007 *Multiple-Scattering Theory: New Developments and Applications* (Cumulative Habilitation, Martin Luther University Halle-Wittenberg)
[25] Lüders M, Ernst A, Temmerman W M, Szotek Z and Durham P J 2001 *J. Phys.: Condens. Matter* **13** 8587
[26] Perdew J P and Wang Y 1992 *Phys. Rev.* B **45** 13244
[27] Birch F 1947 *Phys. Rev.* **71** 809
[28] Poirier J P 2000 *Introduction to the Physics of the Earth's Interior* 2nd edn (Cambridge: Cambridge University Press)

[29] Rowlands D A, Zhang X G and Gonis A 2008 *Phys. Rev.* B **78** 115119
[30] Mirebeau I, Hennion M and Parette G 1984 *Phys. Rev. Lett.* **53** 687
[31] Gyorffy B L, Stocks G M, Ginatempo G, Johnson D D, Nicholson D M, Pinski F J, Staunton J B and Winter H 1991 *Phil. Trans. R. Soc. Lond.* A **334** 515–26
[32] McLachlan A D, Jenkin J G, Leckey R C G and Liesegang J 1975 *J. Phys. F: Met. Phys.* **5** 2415
[33] Winter H, Durham P J and Stocks G M 1984 *J. Phys. F: Met. Phys.* **14** 1047
[34] Caroli C, Lederer-Rozenblatt D, Roulet B and Saint-James D 1973 *Phys. Rev.* B **8** 4552
[35] Hüfner S, Claessen R, Reinert F, Straub T, Strocov V and Steiner P 1999 *J. Electron Spectrosc. Relat. Phenom.* **100** 191
[36] Stadnik Z M, Purdie D, Baer Y and Lograsso T A 2001 *Phys. Rev.* B **64** 214202
[37] Norris C and Nilsson P 1968 *Solid State Commun.* **6** 649
[38] Hüfner S, Wertheim G K and Wernick J H 1973 *Phys. Rev.* B **8** 4511
[39] Hüfner S, Wertheim G and Wernick J 1975 *Solid State Commun.* **17** 1585
[40] Chae K, Lee Y, Whang C, Jeon Y, Choi B and Croft M 1996 *Nucl. Instrum. Methods Phys. Res.* B **117** 123
[41] Tarditi A, Bosko M and Cornaglia L 2012 *Int. J. Hydrog. Energy* **37** 6020